

Article

On Stability of High-Surface-Area Al₂O₃, TiO₂, SiO₂-Al₂O₃, and Activated Carbon Supports during Preparation of NiMo Sulfide Catalysts for Parallel Deoxygenation of Octanoic Acid and Hydrodesulfurization of 1-Benzothiophene

Luděk Kaluža ^{1,*} , Karel Soukup ¹ , Martin Koštein ¹, Jindřich Karban ¹ , Radostina Palcheva ², Marek Laube ¹ and Daniela Gulková ¹

¹ Institute of Chemical Process Fundamentals, Czech Academy of Sciences, Rozvojová 135, 165 02 Prague, Czech Republic

² Institute of Catalysis, Bulgarian Academy of Sciences, Akad. G. Bonchev Str., Bl. 11, 1113 Sofia, Bulgaria

* Correspondence: kaluza@icpf.cas.cz; Tel.: +420-220390270; Fax: +420-220920661

Abstract: NiMo sulfide catalysts were prepared by the impregnation of high surface area supports with an aqueous solution made of NiCO₃·2Ni(OH)₂, MoO₃ and citric acid, followed by freeze drying and sulfidation in H₂S/H₂ mixture. N₂ physisorption and X-ray diffraction were selected to investigate the amphoteric oxides Al₂O₃ and TiO₂, acidic SiO₂-Al₂O₃ and activated carbon supports, fresh prepared sulfide NiMo catalysts and spent catalysts after model parallel reaction of octanoic acid deoxygenation and 1-benzothiophene hydrodesulfurization. The studied mesoporous amphoteric oxides Al₂O₃ and TiO₂ did not lead to highly active NiMo catalysts due to the low hydrothermal stability of these supports during the preparation of the active sulfide phase and deoxygenation reaction. The most active catalyst based on oxidic support was the NiMo sulfide supported on acidic mesoporous SiO₂-Al₂O₃, which was explained by the increased stability of this support to the water and CO/CO₂ mixture during the activation of the sulfidic phase and deoxygenation reaction. The extraordinarily high stability of the activated carbon support led to outstanding activities of the sulfidic NiMo/C catalyst.

Keywords: deoxygenation; hydrodesulfurization; NiMo catalyst; NiMo sulfides; support; activated carbon



Citation: Kaluža, L.; Soukup, K.; Koštein, M.; Karban, J.; Palcheva, R.; Laube, M.; Gulková, D. On Stability of High-Surface-Area Al₂O₃, TiO₂, SiO₂-Al₂O₃, and Activated Carbon Supports during Preparation of NiMo Sulfide Catalysts for Parallel Deoxygenation of Octanoic Acid and Hydrodesulfurization of 1-Benzothiophene. *Catalysts* **2022**, *12*, 1559. <https://doi.org/10.3390/catal12121559>

Academic Editors: Zhongzheng Zhang and Jia Liu

Received: 7 November 2022

Accepted: 28 November 2022

Published: 2 December 2022

Publisher's Note: MDPI stays neutral with regard to jurisdictional claims in published maps and institutional affiliations.



Copyright: © 2022 by the authors. Licensee MDPI, Basel, Switzerland. This article is an open access article distributed under the terms and conditions of the Creative Commons Attribution (CC BY) license (<https://creativecommons.org/licenses/by/4.0/>).

1. Introduction

Modern refining calls for the hydrotreating of synthetic crude coming from waste plastic or renewables to reduce the environmental concerns of using fossil petroleum. These novel feeds bring into the hydrocarbon pool a high oxygen content of up to about 38 wt.% [1–3], mainly in the form of –OH or –COOH groups and their derivatives. During co-hydrotreating of synthetic or renewable feeds with fossil-based feeds, sulfide hydrotreating catalysts face extensive an hydrodeoxygenation (HDO) reaction in addition to an hydrodesulfurization (HDS) reaction. For this reason, the co-hydrotreating of Co(Ni)Mo [4–16], Ru [17], Re [18], or Pt [19,20] catalysts has been studied using feeds containing pyrolyzed biooils [4–12,17,18] or vegetable oils [13–16,19] together with thiophene derivatives [4–8,18] or petroleum fractions [9–16,19].

We have found in our previous work comparing MgO, C, ZrO₂, TiO₂, Al₂O₃, and MCM-41 supports [21] that the sulfidic NiMo phase on each support exhibited systematically higher HDO and HDS activity than the sulfidic CoMo and Mo phase. Nevertheless, this NiMo phase did not lead to highly active catalysts in HDO if it was supported on the amphoteric and basic oxides Al₂O₃, ZrO₂ and MgO, respectively. The inhibition effect of water or CO/CO₂ during HDO that had been reported previously [11,22–27] could explain this observation.

This inhibition principally occurs by two manners, either by destruction of the support or by poisoning of the active NiMoS phase.

First, the support structure and texture are destroyed by water. This phenomenon appeared obvious for high-surface-area MgO support [28,29] but it was also described for γ -Al₂O₃-supported NiMoS [23]. Gamma-alumina recrystallized to hydrous alpha-boehmite phase after treatment with water in the temperature region 140–380 °C. These structural changes were recorded by X-ray diffraction (XRD) and were accompanied with about a 26% decrease in specific surface area (S_{BET}) [23].

Secondly, the active NiMoS phase suffers from partial oxidation. This oxidation mostly happens on the Ni that decorates the edges of the MoS₂ slabs during HDO treatment. This Ni is considered as the most labile but the most active in HDO/HDS. Formation of nickel sulfates, oxides or migration of this labile nickel to form inactive nickel aluminates explains the activity losses [23]. Other inhibition can be due to the adsorption of CO/CO₂ on NiMoS active sites [11]. CO/CO₂ is formed by the decarbonylation and hydrodecarboxylation reactions during HDO. Moreover, CO/CO₂ undergoes water–gas shift and methanation reactions at typical operation conditions of sulfidic NiMo catalysts, which slows down the intrinsic HDO/HDS [26]. Thus, avoiding decarbonylation and hydrodecarboxylation reactions during HDO is recommended [26,30].

The aim of the present work is to investigate the first means of HDO/HDS catalysts deactivation, i.e., the structural and textural changes of the support. The high-surface-area and mesoporous Al₂O₃, TiO₂, SiO₂-Al₂O₃ supports have been selected to deposit NiMo sulfides for parallel reactions of octanoic acid HDO and 1-benzothiophene HDS at 1.6 MPa and 330 °C. The high surface area of the mesopores should be able to disperse the high loading of the NiMo phase. The thin walls of these mesoporous supports should be more sensitive to destruction by H₂O and/or an acidic CO₂/H₂O mixture during reduction sulfidation of catalysts' precursors and/or the HDO/HDS. Activated carbon has been selected due to its inertness and high HDO/HDS activity [21] for the matter of comparison. We therefore elucidated the structural and textural properties of the supports, sulfide catalysts and sulfide catalysts after the HDO/HDS using XRD and nitrogen physisorption, respectively.

2. Results and Discussion

2.1. Structural Characteristics

X-ray diffraction patterns of the studied supports are provided in Figure 1. High-surface-area TiO₂ was notably anatase (PDF 00-021-1272) while other supports were practically X-ray amorphous. Al₂O₃ exhibited broad peaks typical for its gamma phase.

After catalyst preparation, the X-ray patterns showed typical broad and low intensity peaks at about 33.5 (with a shoulder up to about 38) and 58.5 degrees that pointed on the presence of an X-ray amorphous phase of NiMo sulfides in all catalysts. Quite recently [31], the combination of Debye function analysis (DFA) applied to XRD data and high-resolution transmission electron microscopy (HRTEM) explained how these broad and low intensity peaks can be interpreted by the presence of nanocrystallites of MoS₂. The larger shoulder at about 38 degrees was assigned to the presence of multilayers and therefore larger nanocrystallites of MoS₂ [31]. This shoulder can be observed in our Al₂O₃- and TiO₂-supported catalysts. However, it should be noted that the phase of anatase could also explain this shoulder in the TiO₂-supported catalyst. For other catalysts, this shoulder is less pronounced compared to the intensity of the first peak at about 33.5 degrees.

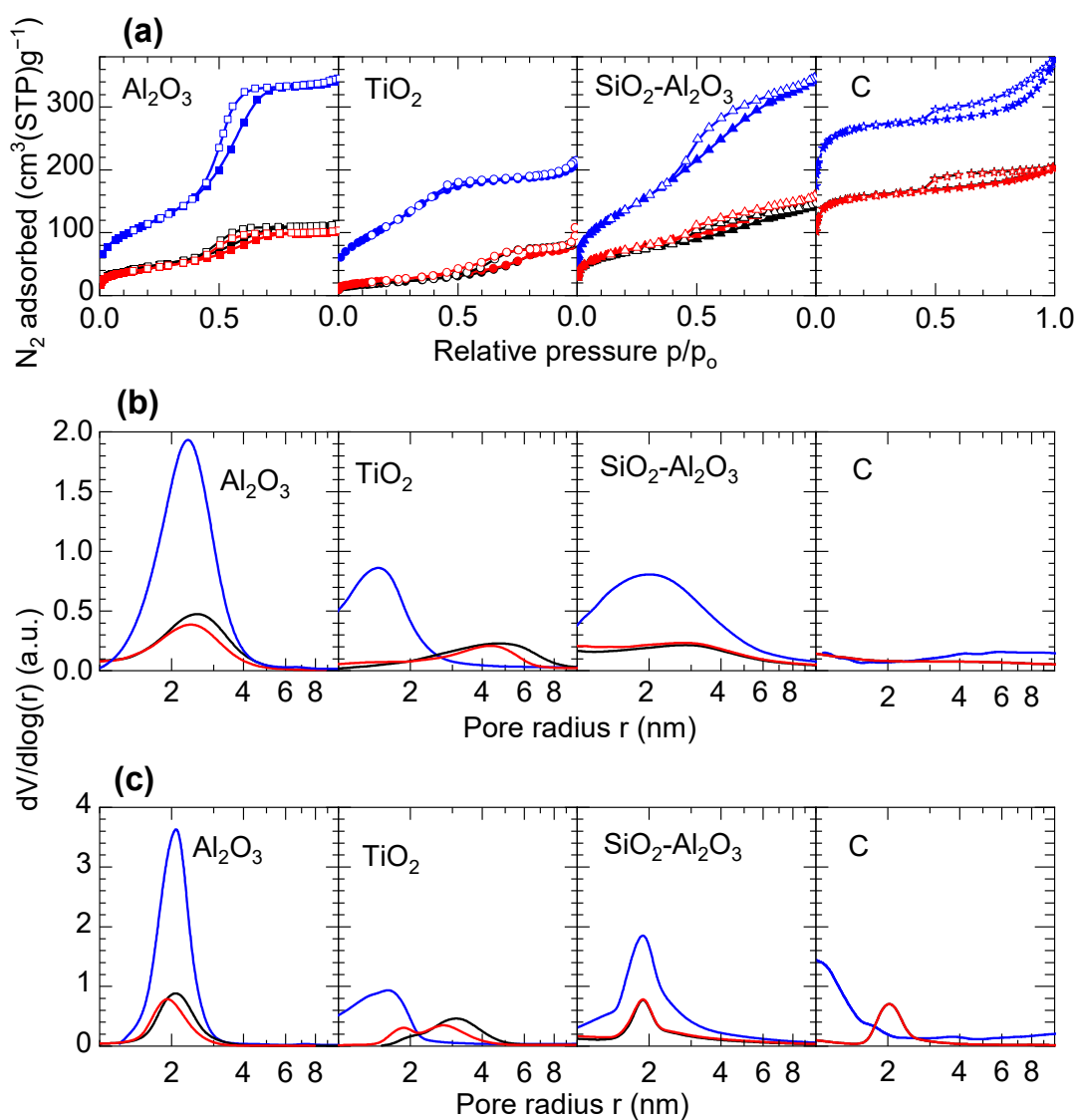


Figure 2. Textural properties of the support (blue lines), sulfided catalysts (black lines) and spent catalysts after 3 h time of stream at 50% conversion of octanoic acid (red lines). N₂ adsorption-desorption isotherms (a), pore-size distribution from the adsorption branch of the isotherm (b), and pore-size distribution from the desorption branch of the isotherm (c).

All supports exhibited S_{BET} higher than 400 m² g⁻¹. Nevertheless, the oxidic supports possessed adsorption–desorption isotherms of type IV typical for materials containing mesopores while activated carbon was highly microporous with the isotherm of type I [32]. In order to quantify the inner surface area of the mesopores, S_M , and the volume of micropores, V_M , a t -plot analysis was done. The results are shown in Table 2. It was ascertained that practically all of the inner surface area of the oxidic supports was located in the mesopores ($S_{BET} \approx S_M$). In contrast, the surface area of the mesopores of the activated carbon S_M represented only about 24% of total S_{BET} . The rest of this rather overestimated value of S_{BET} originated from N₂ sorption in the micropores with pore radii lower than 1 nm.

The following order of increasing mesopore surface area S_M was found within the support studied: C < Al₂O₃ = TiO₂ < SiO₂-Al₂O₃.

Table 2. The comparison of specific surface area S_{BET} with mesopore surface area S_M and volume of micropores V_M normalized per gram of sample (S_M and V_M calculated by t -plot method).

	Support			Fresh Catalyst			Spent Catalyst ^a		
	S_{BET} $m^2 g^{-1}$	S_M $m^2 g^{-1}$	V_M $mm^3 g^{-1}$	S_{BET} $m^2 g^{-1}$	S_M $m^2 g^{-1}$	V_M $mm^3 g^{-1}$	S_{BET} $m^2 g^{-1}$	S_M $m^2 g^{-1}$	V_M $mm^3 g^{-1}$
Al ₂ O ₃	413	399	2	165	164	2	154	143	4
TiO ₂	417	415	<1	72	72	<1	86	86	<1
SiO ₂ - Al ₂ O ₃	500	500	<1	239	205	15	257	229	11
C	919	224	336	517	140	194	515	139	193

^a after 3 h time on stream at 50% conversion of octanoic acid.

2.2.2. NiMo Sulfide Catalysts

Deposition of the NiMo phase using an aqueous solution of citric acid followed by freeze-drying and sulfidation at 400 °C decreased the surface area S_{BET} of the catalysts in comparison with the S_{BET} of the parent supports. The surface area S_{BET} of the sulfided catalysts were also normalized per unit weight of the support in Table 1, assuming the composition of the sulfidic phase NiS-MoS₂, its content in the sulfided catalyst equal to 40 wt.%, and its inherent surface area as negligible. The S_{BET} normalized in this way decreased by about 33, 71, 20, and 6% for the Al₂O₃-, TiO₂-, SiO₂-Al₂O₃-, and C-supported catalyst, respectively. If the inherent surface area of NiS-MoS₂ nanocrystallites is not negligible, then this decrease in S_{BET} would be higher. Clearly, this decrease in the S_{BET} was significant for the Al₂O₃ and TiO₂ supports while it was low for the SiO₂-Al₂O₃ and C. In addition to the significant decrease in S_{BET} and S_M in Table 2, the studied TiO₂ exhibited complex changes in pore-size distribution in Figure 2. Possible changes in the dispersion of NiMo sulfides (Figure 1) necessarily connected with changes in S_{BET} and other textural parameters hardly explain these high differences between the two groups of supports. We concluded that the SiO₂-Al₂O₃ represented the most stable support within the studied high-surface-area and mesoporous oxides. The activated carbon then exhibited extraordinary stability despite being microporous.

The explanation of this high stability of the SiO₂-Al₂O₃ surface lays in the fact that SiO₂-Al₂O₃ endures the reaction with water or CO/CO₂ that is formed during reduction–sulfidation of the deposited complex of Ni, Mo and CA. In contrast, the Al₂O₃ and TiO₂ surface is prone to hydrothermal deterioration. The complex of Ni, Mo and CA does not cover the entire support surface as was the case with the MoO₃ monolayer in our previous works [33–35]. This surface (not covered by Mo) can react with the reaction water from the reduction–sulfidation or CO/CO₂ originated from the citric acid, which causes the partial destruction of pore walls and a decrease in the S_{BET} . The activated carbon is inert towards this type of chemical deterioration.

2.3. Catalytic Activity

Table 1 summarizes the activities k_{HDO} and k_{HDS} of the prepared catalysts in the HDO/HDS reaction. The fitting of k_{HDO} and k_{HDS} by Equations (1) and (2) is shown in Figure 3.

The high-surface-area Al₂O₃ resulted in the catalyst with the lowest HDO and HDS activity. The TiO₂-supported catalyst exhibited increased HDO activity while HDS activity remained low. It should be noted that these activities are lower than those achieved previously [21] over conventional γ -Al₂O₃ ($S_{BET} = 262 m^2 g^{-1}$) and TiO₂ (anatase, $S_{BET} = 140 m^2 g^{-1}$) carriers. In our previous study [21], the NiMo sulfidic catalysts possessed k_{HDO} and k_{HDS} 105 and 128 mmol g⁻¹ h⁻¹ for the γ -Al₂O₃ and 275 and 90 mmol g⁻¹ h⁻¹ for the anatase, respectively. The unprecedentedly low activities reached currently over the high-surface-area and mesoporous Al₂O₃ and TiO₂ can be explained by the complete textural collapse of these supports during catalyst preparation.

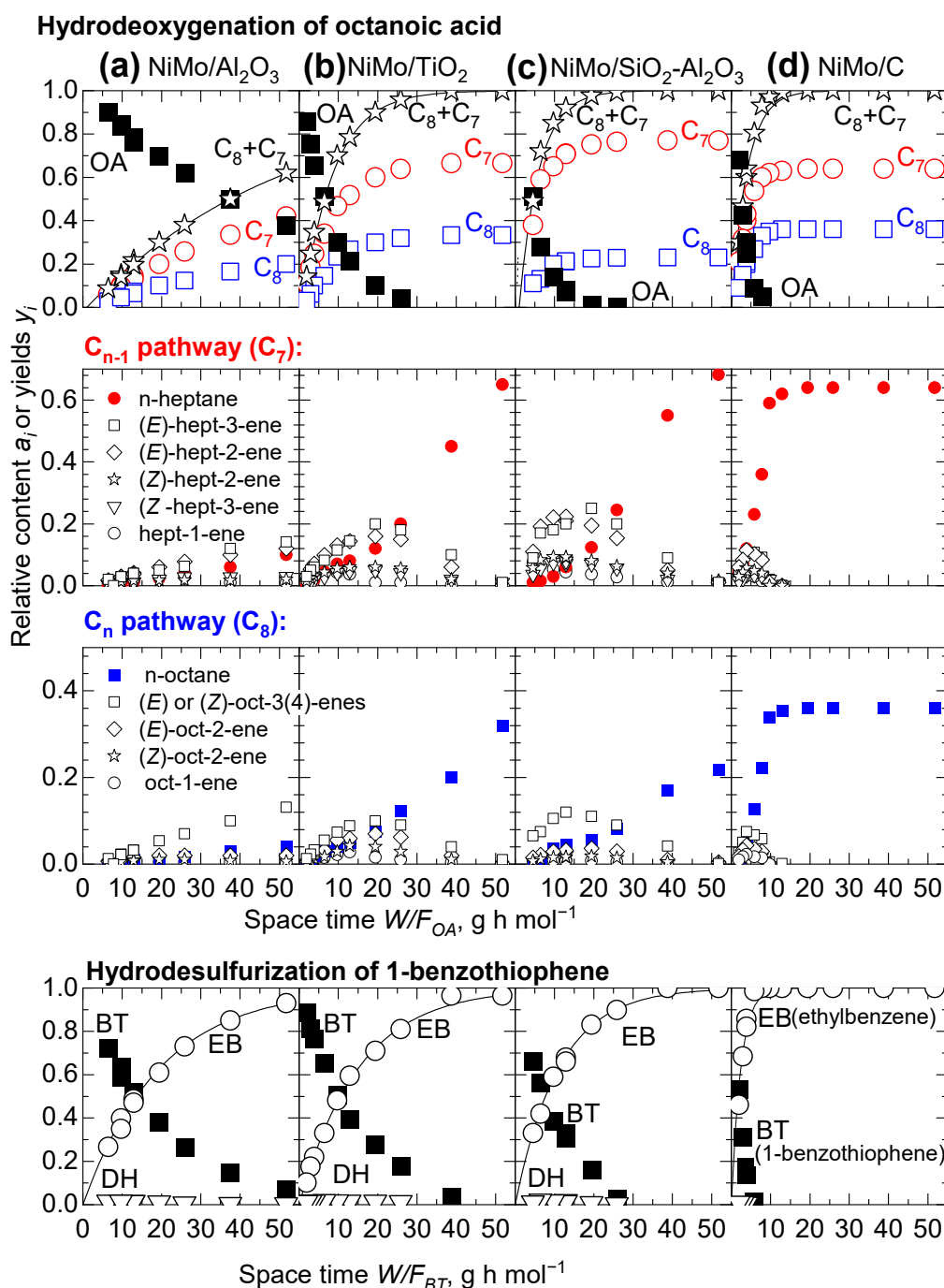


Figure 3. The formation of linear C₈ and C₇ hydrocarbons and ethylbenzene (EB) during parallel HDO/HDS of octanoic acid (OA) and 1-benzothiophene (BT) over the studied catalysts: solid lines—fitting of activity k_{HDO} and k_{HDS} by Equations (1) and (2), respectively.

In contrast, the SiO₂-Al₂O₃-supported NiMo catalyst exhibited the highest activities in HDO and HDS comparing the studied mesoporous oxidic supports, which well correlates with the highest S_{BET} given in Table 1 and other textural parameters summarized in Table 2 and Figure 2. Nevertheless, the activated carbon had the most inert surface to hydrothermal deterioration during the preparation of NiMo sulfides, which resulted in the most active catalyst within the studied series. The presented high k_{HDO} and k_{HDS} corroborated previously published results [21] that were achieved over similar activated carbon (product no. GA05) and the NiMo phase. The activated carbon thus remains the most promising support resulting in extraordinary high HDO/HDS activities.

2.4. Textural Stability during HDO/HDS Reactions

Tables 1 and 2 and Figure 2 also show how the studied textural parameters of the catalysts differed after 3-h time on stream. We hardly found significant changes in textural parameters or HDO/HDS activities after this simplified deactivation test. Clearly, the studied catalysts were stable during the HDO/HDS experiment. The most significant changes in textural properties thus took place during the preparation of the catalysts including the reduction–sulfidation procedure as was discussed above. The water, CO, or CO₂ that are produced during the HDO did not continue the deterioration of the textural properties, which could be explained by the low partial pressure of these inhibitors.

2.5. Selectivity in HDO/HDS Reactions

2.5.1. HDO/HDS Selectivity

Table 1 shows that NiMo/Al₂O₃ (the least active catalyst) and NiMo/C (the most active catalyst) were less selective to HDO than to HDS while NiMo/TiO₂ and NiMo/SiO₂-Al₂O₃ were about two times more selective to HDO than to HDS. The explanation of this HDO/HDS selectivity behavior has been previously found in empiric correlation with the point of zero charge, PZC, of the support [21]. The amphoteric supports with PZC about 7 result in NiMo catalysts with low selectivity to HDO. This is the case of the studied Al₂O₃ and activated carbon. In contrast, slightly more acidic TiO₂ with PZC about 5 and the SiO₂-Al₂O₃ with PZC about 4.5 are more selective to HDS. In summary, the hydrothermal inertness of the surface of the activated carbon leading to preservation of the catalyst texture and low metal-support interactions resulted in extraordinarily high HDO and HDS activities in the NiMo/C compared with the NiMo/SiO₂-Al₂O₃.

2.5.2. Selectivity to Reaction Intermediates

In contrast to HDO/HDS selectivity, the selectivities to reaction intermediates during HDO/HDS reactions were similar over all of the prepared catalysts as shown in Figure 3.

No octanol was observed during the HDO of octanoic acid. The formation of olefins, the intermediates of the HDO reaction, was pronounced at low space time while hydrogenation to n-octane and n-heptane predominated at higher space time. We observed the same in our previous work over NiMo sulfides supported on commercial carriers [21].

The C_{n-1} pathway (decarboxylation/decarbonylation) yielding C₇ olefins and finally n-heptane predominated over all catalysts. The C_n pathway (intrinsic hydrodeoxygenation) yielding C₈ olefins and finally n-octane was less pronounced. The Al₂O₃-, TiO₂-, and C-supported NiMo catalysts yielded about 67% of C₇ hydrocarbons (from total yield of hydrocarbons) while the SiO₂-Al₂O₃-supported NiMo catalyst yielded about 75% of C₇ hydrocarbons. We did not observe any cracking (C_{n-x} pathway). The acidity of SiO₂-Al₂O₃ containing 25 wt.% of Al₂O₃ was thus lower than that of the MCM-41 in our previous paper [21]. The formation of branched hydrocarbons such as 2-methyl-hexane, 3-methyl-hexane, 2-(or 4)-methyl-heptane, and 3-methyl-heptane was observed only over the SiO₂-Al₂O₃-supported NiMo catalyst, but within amounts lower than 2% of C₈ + C₇ yields, and so it was not shown in Figure 3.

The formation of dihydrobenzothiophene (DH), the reaction intermediate of 1-benzothiophene HDS, was negligible over all catalysts.

Figure 3 clearly shows that the hydrogenation function of the NiMo/C catalyst is predominant because the presence of linear olefins is the least pronounced within the studied catalysts.

2.6. Recapitulative Discussion and Outlook

The present contribution touched on important aspects for the forthcoming research of HDO/HDS catalysts:

- The method of catalyst preparation should be tailored to the specific character of each individual support.

- The properly used chelating agent leads to highly active catalysts containing a variety of supports including Al₂O₃ [31,36,37] but it appeared detrimental for the studied high surface area Al₂O₃ and TiO₂.
- The supports on the base of SiO₂-Al₂O₃ represent a promising alternative to single oxides because they could be tuned in a wide range of acid-base properties [38–44] and because they increase dispersion of MoS₂ compared to SiO₂ [37]. Acidity seems crucial for the HDO of fatty acid containing feeds because it influences the formation of linear or branched hydrocarbons [21,41].
- The active phase should hydrogenate olefins, the reaction intermediates of the HDO of fatty-acid-containing feeds. In this respect, the most promising support of the NiMo phase was found to be the activated carbon. Activated carbon as well as the use of citric acid contributes to low metal-support interaction and stability of Type II NiMoS phase containing a high number of corner sites [36,37].
- The active phase and mesoporous support should provide stability to water and CO/CO₂ that has not been needed to such an extent in a single HDS reaction [28,34,35,45–49].

3. Materials and Methods

The Al₂O₃ and SiO₂-Al₂O₃ were synthesized by previously reported methods [33] and [50], respectively. SiO₂-Al₂O₃ contained 25 wt.% of Al₂O₃, which was found optimal to achieve high HDS activity [51]. TiO₂ was a commercial support (NanoScale Materials Inc., Manhattan, KA, USA, Product No. AC312-0100). Activated carbon, C, was a commercial support (Slovenské lučobné závody a.s., Hnúšťa, Slovakia, Product No. GA1). All supports were uniformized to particle size fraction 0.16–0.32 mm by grinding and sieving.

The impregnation solution was prepared by dissolution of NiCO₃·2Ni(OH)₂ (Sigma-Aldrich Chemie GmbH, Steinheim, Germany, Product No. 544183), MoO₃ (Sigma-Aldrich Chemie GmbH, Steinheim, Germany, Product No. 69850) and citric acid, CA, (Lach-Ner s.r.o., Neratovice, Czechia, Product No. 10019-AP0) in water. The molar ratio of Ni:Mo:CA was 1.00:2.33:3.33. The support with impregnation solution was stirred for 15 min at laboratory temperature, cooled in liquid nitrogen for 1 min and dried in a freeze-dryer for 3 days. Freeze drying was chosen to lessen the interaction of Mo species with the support to form undesirable three dimensional heteropolymolybdates [52]. The relatively long 3-day freeze-drying time is necessary to remove moisture from the pores of the supports. We verified on part of the samples that an additional drying in a conventional oven at 110 °C did not lead to any weight loss. The samples removed from the freeze dryer were immediately sulfided in a gaseous H₂S:H₂ mixture (1:10) at 400 °C for 1 h. The catalysts were stored in gas tight ampules under N₂. Chemical analysis by atomic absorption spectroscopy, AAS, confirmed the same content of Mo and Ni in all catalysts (19.0 ± 0.5 wt.% Mo and 5.0 ± 0.3 wt.% Ni).

X-ray diffraction measurements, XRD, were done on Bruker D8 Advanced Eco Powder X-ray analyzer (Bruker Corporation, Karlsruhe, Germany) with filtered CuK α radiation at 40 kV acceleration and 25 mA current of the X-ray tube, scan step 0.02° and 4 s accumulation time at each step. Physisorption of N₂ was performed over the supports and catalysts on an ASAP 2020 Micromeritics instrument (Micromeritics Instrument Corporation, Norcross, GE, USA) after degassing at 350 °C and 1 Pa vacuum for 24 h. The adsorption–desorption isotherms of nitrogen at 77 K were evaluated by the standard Brunauer–Emmett–Teller procedure [53] for the p/p⁰ range = 0.05–0.25 to calculate the specific surface area S_{BET} . The pore-size distribution (pore radius 1–10 nm) was evaluated from both the adsorption and desorption branch of N₂ isotherm by the Barrett–Joyner–Halenda (BJH) method [54] assuming a cylindrical pore geometry. The Lecloux–Pirard standard isotherm [55] was used for the *t*-plot and for the pore-size distribution evaluation. Volume of micropores, V_M , and surface area of mesopores, S_M , were also determined [56]. The determination of S_{BET} , S_M , and V_M were made with an accuracy of ±5%.

The activity of catalyst in parallel HDO/HDS of octanoic acid (OA)/1-benzothiophene (BT) was determined by the previously reported method [21] in laboratory-scale tubular flow reactor at 330 °C and 1.6 MPa. The catalyst weight, W , was 0.1, 0.2 and 0.4 g. The NiMo/C was additionally measured at weight 0.03 g due to its high activity; as reported therein. The reaction was run at three feed rates, F , of OA and BT: 7.7 mmol h⁻¹, 10.3 mmol h⁻¹, and 15.5 mmol h⁻¹. The pseudo-first order rate constant, k_{HDO} , of C₈ + C₇ hydrocarbons formation, y_{C8+C7} , during the HDO of OA and the pseudo-first order rate constant, k_{HDS} , of ethylbenzene (EB) formation, y_{EB} , during the HDS of BT was fitted by non-linear regression and used as the index of catalyst activity:

$$y_{C8+C7} = 1 - \exp(-k_{HDO} \times W/F_{OA}) \quad (1)$$

$$y_{EB} = 1 - \exp(-k_{HDS} \times W/F_{BT}) \quad (2)$$

In addition to this activity test [21], the catalysts were also compared at relative yields of C₈ + C₇ hydrocarbons $y_{C8+C7} = 0.5$ in terms of stability. The yield $y_{C8+C7} = 0.5$ was achieved at 50% conversion of OA. The catalysts were taken from the reactor after 3-h time on stream and their textural properties were characterized by N₂ physisorption. The determination of k_{HDO} and k_{HDS} were made with an accuracy of ±10%.

4. Conclusions

The co-impregnation of the high-surface-area mesoporous Al₂O₃ and TiO₂ supports with aqueous solution of NiCO₃·2Ni(OH)₂, MoO₃ and citric acid, followed by freeze drying and reduction–sulfidation resulted in catalysts of low surface area and low activities in hydrodeoxygenation of octanoic acid and hydrodesulfurization of 1-benzothiophene. In contrast, this method of preparation was successful for the high-surface-area SiO₂-Al₂O₃ support containing 25 wt.% of Al₂O₃ and the activated carbon. The BET area of the sulfidic NiMo/SiO₂-Al₂O₃ catalyst with Ni and Mo contents of 5 and 20 wt.%, respectively, was 240 m² g⁻¹. This surface area practically represents the surface area of the mesopores and it remained the same after the HDO/HDS reaction. This catalyst mostly yielded linear hydrocarbons by HDO convenient for diesel fuel and it also exhibited high activity in HDS. Nevertheless, the most active catalyst in both HDO and HDS was NiMo/C. At the same loading of NiMo, the mesopore surface area was only about 140 m² g⁻¹ due to high microporosity of the activated carbon. The textural stability of the activated carbon towards the hydrothermal deterioration during the reduction–sulfidation step of catalyst preparation was the highest among the studied supports.

Author Contributions: Conceptualization, writing and funding acquisition, L.K.; methodology K.S.; investigation, M.K.; data curation, J.K.; resources, R.P., formal analysis, M.L.; visualization, D.G. All authors have read and agreed to the published version of the manuscript.

Funding: This research was funded by the Czech Science Foundation grant no. 17-22490S, the Technology Agency of the Czech Republic grant No. TN01000048 and mobility project CAS-BAS grant no. BAS-20-01.

Data Availability Statement: Not applicable.

Acknowledgments: The senior scientists M. Zdražil and O. Šolcová are acknowledged for their help with reaction progress kinetic analysis (RPKA) and textural analysis (BET, BJH), respectively.

Conflicts of Interest: The authors declare no conflict of interest.

References

1. Furimsky, E. Catalytic hydrodeoxygenation. *Appl. Catal. A* **2000**, *199*, 147–190. [[CrossRef](#)]
2. Mortensen, P.M.; Grunwaldt, J.D.; Jensen, P.A.; Knudsen, K.G.; Jensen, A.D. A review of catalytic upgrading of bio-oil to engine fuels. *Appl. Catal. A* **2011**, *407*, 1–19. [[CrossRef](#)]
3. Furimsky, E. Hydroprocessing challenges in biofuels production. *Catal. Today* **2013**, *217*, 13–56. [[CrossRef](#)]

4. Platanitis, P.; Panagiotou, G.D.; Bourikas, K.; Kodulis, C.; Lycourghiotis, A. Hydrodeoxygenation of phenol over hydrotreatment catalysts in their reduced and sulfided states. *Open Catal. J.* **2014**, *7*, 18–25. [[CrossRef](#)]
5. Xia, L.; Xia, Z.; Tang, W.; Wang, H.; Fang, M. Hydrogenation of Model Compounds Catalyzed by MCM-41-Supported Nickel Phosphide. *Adv. Mater. Res.* **2014**, *864–867*, 366–372. [[CrossRef](#)]
6. Wang, W.; Zhu, G.; Li, L.; Tan, S.; Wu, K.; Zhang, X.; Yang, Y. Facile hydrothermal synthesis of flower-like Co–Mo–S catalysts and their high activities in the hydrodeoxygenation of p-cresol and hydrodesulfurization of benzothiophene. *Fuel* **2016**, *174*, 1–8. [[CrossRef](#)]
7. Dhandapani, B.; Clair, T.; Oyama, S.T. Simultaneous hydrodesulfurization, hydrodeoxygenation, and hydrogenation with molybdenum carbide. *Appl. Catal. A* **1998**, *168*, 219–228. [[CrossRef](#)]
8. Odebunmi, E.O.; Ollis, D.F. Catalytic hydrodeoxygenation: II. Interactions between catalytic hydrodeoxygenation of m-cresol and hydrodesulfurization of benzothiophene and dibenzothiophene. *J. Catal.* **1983**, *80*, 65–75. [[CrossRef](#)]
9. Pstrowska, K.; Walendziewski, J.; Łuzny, R.; Stolarski, M. Hydroprocessing of rapeseed pyrolysis bio-oil over NiMo/Al₂O₃ catalyst. *Catal. Today* **2014**, *223*, 54–65. [[CrossRef](#)]
10. Pstrowska, K.; Walendziewski, J.; Stolarski, M. Hydrorefining of oil from rapeseed cake pyrolysis over NiMo/Al₂O₃ catalyst. *Fuel Process. Technol.* **2014**, *128*, 191–198. [[CrossRef](#)]
11. Pinheiro, A.; Hudebine, D.; Dupassieux, N.; Geantet, C. Impact of oxygenated compounds from lignocellulosic biomass pyrolysis oils on gas oil hydrotreatment. *Eng. Fuel.* **2009**, *23*, 1007–1014. [[CrossRef](#)]
12. Bui, V.N.; Toussaint, G.; Laurenti, D.; Mirodatos, C.; Geantet, C. Co-processing of pyrolysis bio oils and gas oil for new generation of bio-fuels: Hydrodeoxygenation of guaiacol and SRGO mixed feed. *Catal. Today* **2009**, *143*, 172–178. [[CrossRef](#)]
13. Vonortas, A.; Kubicka, D.; Papayannakos, N. Catalytic co-hydroprocessing of gasoil–palm oil/AVO mixtures over a NiMo/ γ -Al₂O₃ catalyst. *Fuel* **2014**, *116*, 49–55. [[CrossRef](#)]
14. Varakin, A.N.; Salnikov, V.A.; Nikulshina, M.S.; Maslakov, K.I.; Mozhaev, A.V.; Nikulshin, P.A. Beneficial role of carbon in Co(Ni)MoS catalysts supported on carbon-coated alumina for co-hydrotreating of sunflower oil with straight-run gas oil. *Catal. Today* **2017**, *292*, 110–120. [[CrossRef](#)]
15. Nikulshin, P.A.; Salnikov, V.A.; Pimerzin, A.A.; Eremina, Y.V.; Koklyukhin, A.S.; Tsvetkov, V.S.; Pimerzin, A.A. Co-hydrotreating of straight-run diesel fraction and vegetable oil on Co(Ni)-PMo/Al₂O₃ catalysts. *Petrol. Chem.* **2016**, *56*, 56–61. [[CrossRef](#)]
16. Eller, Z.; Varga, Z.; Hancsók, J. Renewable Jet Fuel from Kerosene/Coconut Oil Mixtures with Catalytic Hydrogenation. *Energ. Fuel.* **2019**, *33*, 6444–6453. [[CrossRef](#)]
17. Mercader, F.M.; Groeneveld, M.J.; Kersten, S.R.A.; Geantet, C.; Toussaint, G.; Way, N.W.J.; Schaverien, C.J.; Hogendoorn, K.J.A. Hydrodeoxygenation of pyrolysis oil fractions: Process understanding and quality assessment through co-processing in refinery units. *Eng. Environ. Sci.* **2011**, *4*, 985–997.
18. Sepúlveda, C.; Escalona, N.; García, R.; Laurenti, D.; Vrinat, M. Hydrodeoxygenation and hydrodesulfurization co-processing over ReS₂ supported catalysts. *Catal. Today* **2012**, *195*, 101–105. [[CrossRef](#)]
19. Vonortas, A.; Papayannakos, N. Hydrodesulfurization and hydrodeoxygenation of gasoil-vegetable oil mixtures over a Pt/ γ -Al₂O₃ catalyst. *Fuel Process. Technol.* **2016**, *150*, 126–131. [[CrossRef](#)]
20. Morales-Hernández, G.; Pacheco-Sosa, J.G.; Escobar-Aguilar, J.; Torres, J.G.T.; Pérez-Vidal, H.; Lunagómez-Rocha, M.A.; De La Cruz-Romero, D.; Del Ángel-Vicente, P. Improving platinum dispersion on sba-15 by titania addition. *Rev. Mex. Ing. Quim.* **2020**, *19*, 997–1010. [[CrossRef](#)]
21. Kaluža, L.; Karban, J.; Gulková, D. Activity and selectivity of Co(Ni)Mo sulfides supported on MgO, Al₂O₃, ZrO₂, TiO₂, MCM-41 and activated carbon in parallel hydrodeoxygenation of octanoic acid and hydrodesulfurization of 1-benzothiophene. *Reac. Kinet. Mech. Cat.* **2019**, *127*, 887–902. [[CrossRef](#)]
22. Yoshimura, Y.; Sato, T.; Shimada, H.; Matsubayashi, N.; Nishijima, A. Influences of oxygen-containing substances on deactivation of sulfided molybdate catalysts. *Appl. Catal.* **1991**, *73*, 55–63. [[CrossRef](#)]
23. Laurent, E.; Delmon, B. Influence of water in the deactivation of a sulfided NiMo γ -Al₂O₃ catalyst during hydrodeoxygenation. *J. Catal.* **1994**, *146*, 281–291. [[CrossRef](#)]
24. Li, Y.; Wang, R.; Chang, L. Study of reactions over sulfide catalysts in CO–CO₂–H₂–H₂O system. *Catal. Today* **1999**, *51*, 25–38. [[CrossRef](#)]
25. Senol, O.I.; Viljava, T.R.; Krause, A.O.I. Hydrodeoxygenation of aliphatic esters on sulphided NiMo/ γ -Al₂O₃ and CoMo/ γ -Al₂O₃ catalyst: The effect of water. *Catal. Today* **2005**, *106*, 186–189.
26. Pinheiro, A.; Dupassieux, N.; Hudebine, D.; Geantet, C. Impact of the Presence of Carbon Monoxide and Carbon Dioxide on Gas Oil Hydrotreatment: Investigation on Liquids from Biomass Cotreatment with Petroleum Cuts. *Eng. Fuel.* **2011**, *25*, 804–812. [[CrossRef](#)]
27. Coumans, A.E.; Hensen, E.J.M. A model compound (methyl oleate, oleic acid, triolein) study of triglycerides hydrodeoxygenation over alumina-supported NiMo sulfide. *Appl. Catal. B Environ.* **2017**, *201*, 290–301. [[CrossRef](#)]
28. Mejias, J.A.; Berry, A.J.; Refson, K.; Fraser, D.G. The kinetics and mechanism of MgO dissolution. *Chem. Phys. Lett.* **1999**, *314*, 558–563.
29. Klicpera, T.; Zdražil, M. Preparation of high-activity MgO-supported Co–Mo and Ni–Mo sulfide hydrodesulfurization catalysts. *J. Catal.* **2002**, *206*, 314–320. [[CrossRef](#)]

30. Vlasova, E.N.; Bukhtiyarova, G.A.; Deliy, I.V.; Aleksandrov, P.V.; Porsin, A.A.; Panafidin, M.A.; Gerasimov, E.Y.; Bukhtiyarov, V.I. The effect of rapeseed oil and carbon monoxide on SRGO hydrotreating over sulfide CoMo/Al₂O₃ and NiMo/Al₂O₃ catalysts. *Catal. Today* **2020**, *357*, 526–533. [[CrossRef](#)]
31. Pakharukova, V.P.; Yatsenko, D.A.; Gerasimov, E.Y.; Vlasova, E.; Bukhtiyarova, G.A.; Tsybulya, S.V. Total Scattering Debye Function Analysis: Effective Approach for Structural Studies of Supported MoS₂-Based Hydrotreating Catalysts. *Ind. Eng. Chem. Res.* **2020**, *59*, 10914–10922. [[CrossRef](#)]
32. Gregg, S.J.; Sing, K.S.W. *Adsorption, Surface Area and Porosity*, 2nd ed.; Academic Press: London, UK, 1982; pp. 1–303.
33. Kaluža, L.; Gulková, D.; Šolcová, O.; Žilková, N.; Čejka, J. Hydrotreating catalysts supported on organized mesoporous alumina: Optimization of Mo deposition and promotional effects of Co and Ni. *Appl. Catal. A Gen.* **2008**, *351*, 93–101. [[CrossRef](#)]
34. Kaluža, L.; Zdražil, M.; Žilková, N.; Čejka, J. High activity of highly loaded MoS₂ hydrodesulfurization catalysts supported on organised mesoporous alumina. *Catal. Commun.* **2002**, *3*, 151–157. [[CrossRef](#)]
35. Čejka, J.; Žilková, N.; Kaluža, L.; Zdražil, M. Mesoporous alumina as a support for hydrodesulfurization catalysts. *Stud. Surf. Sci. Catal.* **2002**, *141*, 243–250.
36. Escobar, J.; Barrera, M.C.; Gutiérrez, A.W.; Terrazas, J.E. Benzothiophene hydrodesulfurization over NiMo/alumina catalysts modified by citric acid. Effect of addition stage of organic modifier. *Fuel Process. Technol.* **2017**, *156*, 33–42. [[CrossRef](#)]
37. Hensen, E.J.M.; Kooyman, P.J.; Van der Meer, Y.; Van der Kraan, A.M.; De Beer, V.H.J.; Van Veen, J.A.R.; Van Santen, R.A. The Relation between Morphology and Hydrotreating Activity for Supported MoS₂ Particles. *J. Catal.* **2001**, *199*, 224–235. [[CrossRef](#)]
38. Nguyen, M.T.; Tayakout-Fayolle, M.; Chainet, F.; Pirngruber, G.D.; Geantet, C. Use of kinetic modeling for investigating support acidity effects of NiMo sulfide catalysts on quinoline hydrodenitrogenation. *C. Appl. Catal. A Gen.* **2017**, *530*, 132–144. [[CrossRef](#)]
39. Coumans, A.E.; Hensen, E.J.M. A real support effect on the hydrodeoxygenation of methyl oleate by sulfided NiMo catalysts. *Catal. Today* **2017**, *298*, 181–189. [[CrossRef](#)]
40. Escalona, G.; Rai, A.; Betancourt, P.; Sinha, A.K. Selective poly-aromatics saturation and ring opening during hydroprocessing of light cycle oil over sulfided Ni-Mo/SiO₂-Al₂O₃ catalyst. *Fuel* **2018**, *219*, 270–278. [[CrossRef](#)]
41. Ramesh, A.; Tamizhdurai, P.; Krishnan, P.S.; Ponnusamy, V.K.; Sakthinathan, S.; Shanthi, K. Catalytic transformation of non-edible oils to biofuels through hydrodeoxygenation using Mo-Ni/mesoporous alumina-silica catalysts. *Fuel* **2020**, *262*, 116494. [[CrossRef](#)]
42. Ramesh, A.; Tamizhdurai, P.; Mangesh, V.L.; Palanichamy, K.; Gopinath, S.; Sureshkumar, K.; Shanthi, K. Mg/SiO₂-Al₂O₃ supported nickel catalysts for the production of naphthenic hydrocarbon fuel by hydro-de-oxygenation of eugenol. *Int. J. Hydrogen Energy* **2019**, *44*, 25607–25620. [[CrossRef](#)]
43. Agliullin, M.R.; Danilova, I.G.; Faizullin, A.V.; Amarantov, S.V.; Bubennov, S.V.; Prosochkina, T.R.; Grigoreva, N.G.; Paukshtis, E.A.; Kutepov, B.I. Sol-gel synthesis of mesoporous aluminosilicates with a narrow pore size distribution and catalytic activity thereof in the oligomerization of dec-1-ene. *Micropor. Mesopor. Mat.* **2016**, *230*, 118–127. [[CrossRef](#)]
44. Serrano, D.P.; Escola, J.M.; Briones, L.; Arroyo, M. Selective hydrodecarboxylation of fatty acids into long-chain hydrocarbons catalyzed by Pd/Al-SBA-15. *Micropor. Mesopor. Mat.* **2019**, *280*, 88–96. [[CrossRef](#)]
45. Dzwigaj, S.; Louis, C.; Breyse, M.; Cattenot, M.; Bellière, V.; Geantet, C.; Vrinat, M.; Blanchard, P.; Payen, E.; Inoue, S.; et al. New generation of titanium dioxide support for hydrodesulfurization. *Appl. Catal. B Environ.* **2003**, *41*, 181–191. [[CrossRef](#)]
46. Wang, H.; Xiao, B.; Cheng, X.; Wang, C.; Zhao, L.; Zhu, Y.; Zhu, J.; Lu, X. NiMo catalysts supported on graphene-modified mesoporous TiO₂ toward highly efficient hydrodesulfurization of dibenzothiophene. *Appl. Catal. A Gen.* **2015**, *502*, 157–165. [[CrossRef](#)]
47. Plataniotis, P.; Panagiotou, G.D.; Bourikas, K.; Kordulis, C.; Fierro, J.L.G.; Lycourghiotis, A. Preparation of un-promoted molybdenum HDS catalysts supported on titania by equilibrium deposition filtration: Optimization of the preparative parameters and investigation of the promoting action of titania. *J. Mol. Catal. A Chem.* **2016**, *412*, 1–12. [[CrossRef](#)]
48. Naboulsi, I.; Lebeau, B.; Aponte, C.F.L.; Brunet, S.; Mallet, M.; Michelin, L.; Bonne, M.; Carteret, C.; Blin, J.L. Selective direct desulfurization way (DDS) with CoMoS supported over mesostructured titania for the deep hydrodesulfurization of 4, 6-dimethyldibenzothiophene. *Appl. Catal. A Gen.* **2018**, *563*, 91–97. [[CrossRef](#)]
49. Li, M.; Song, J.; Yue, F.; Pan, F.; Yan, W.; Hua, Z.; Li, L.; Yang, Z.; Li, L.; Wen, G.; et al. Complete Hydrodesulfurization of Dibenzothiophene via Direct Desulfurization Pathway over Mesoporous TiO₂-Supported NiMo Catalyst Incorporated with Potassium. *Catalysts* **2019**, *9*, 448. [[CrossRef](#)]
50. Vít, Z.; Šolcová, O. Synthesis and properties of mesoporous silica–alumina with narrow pore size distribution obtained without use of pore-regulating agents. *Micropor. Mesopor. Mater.* **2006**, *96*, 197–204. [[CrossRef](#)]
51. Kaluža, L.; Gulková, D.; Vít, Z.; Zdražil, M. Water-assisted spreading of MoO₃ onto SiO₂-Al₂O₃ supports for preparation of sulfide CoMo hydrodesulfurization catalysts. *Fuel* **2013**, *112*, 272–276. [[CrossRef](#)]
52. Carrier, X.; Lambert, J.F.; Kuba, S.; Knözinger, H.; Che, M. Influence of ageing on MoO₃ formation in the preparation of alumina-supported Mo catalysts. *J. Mol. Struct.* **2003**, *656*, 231–238. [[CrossRef](#)]
53. Brunauer, S.; Emmett, P.H.; Teller, E. Adsorption of gases in multimolecular layers. *J. Am. Chem. Soc.* **1938**, *60*, 309–319. [[CrossRef](#)]
54. Barrett, E.P.; Joyner, L.G.; Halenda, P.P. The determination of pore volume and area distributions in porous substances. I. Computations from nitrogen isotherms. *J. Am. Chem. Soc.* **1951**, *73*, 373–380.

-
55. Lecloux, A.; Pirard, J.P. The importance of standard isotherms in the analysis of adsorption isotherms for determining the porous texture of solids. *J. Colloid Interface Sci.* **1979**, *70*, 265–281. [[CrossRef](#)]
 56. Schneider, P. Adsorption isotherms of microporous-mesoporous solids revisited. *Appl. Catal. A Gen.* **1995**, *129*, 157–165. [[CrossRef](#)]